**Bruno Naylor** Master 2 Quantum Devices 2012/2013

# Setting up an optical dipole trap and a non destructive *in situ* imaging system for a BEC experiment

Supervised by L.Vernac, E. Maréchal and B.Laburthe-Tolra



# Contents

# List of Figures

# Introduction

The idea of Bose-Einstein condensation dates back to 1925 where A.Einstein, on the basis of a paper by the physicist S.N. Bose, predicted the occurrence of a phase transition in a gas of non-interacting atoms. This phase transition is associated with the condensations of atoms in the state of lowest energy and is the consequence of quantum statistical effects. The experimental studies on dilute atomic gases were developed much later, starting from the 1970s, enabled by the development in atomic physics of new techniques based on magnetic and optical trapping and advanced cooling techniques.

The development of these techniques led to the realisation of a Bose Einstein Condensation (BEC) in 1995. The achievement of BEC, and its early experimental studies, led to the Nobel Prize in Physics in 2001 for E.A Cornell, W. Ketterle, amd C.E. Wieman. The atoms in a BEC have the same quantum mechanical properties and can be treated as one entity. One of the reasons why BECs are so attractive is that they can be observed for seconds, manipulated, shaken, without losing their quantum properties. BEC is therefore one ideal candidate for quantum physics experiments.

After BEC was obtained at JILA in Boulder, and at MIT, with alcaline atoms followed by many others, a chromium BEC was obtained in Stuttgart in 2005 [1]. In 2006 at LPL in Paris, a simultaneous Magneto-Optical Trap (MOT) of Bosonic and Fermionic atoms was produced [2]. While the Fermion species was set aside, and producing a Fermi Sea of chromium will be a main task of my PhD, the bosonic species was condensed in 2008 [3].

The goal of my work was to produce an optical dipole trap for the BEC of $40\mu m$ waist horizontally and $10\mu m$ waist vertically. This configuration should lead to a quasi 2D gas, and should give a BEC's size bigger than the spin healing length in the strong confining direction. This should likely lead to the formation of spin domains which we would like to observe, necessitating the production of a new imaging system capable of observing the atomic spin. In this report, I will explain why chromium was chosen to be condensed and I will present the latest work that the Laboratoire de Physique des Lasers team has produced. Then I shall explain how to create an optical dipole trap and give our optical dipole trap characteristics. Finally I will describe the actual imaging system before a detailed study of the new imaging system which will be in situ, non destructive, and able to probe spin domains.

# 1 Studiying Magnetism with Chromium

Chromium was first condensed [1] 10 years after the first BEC. In this section I will introduce the main properties of chromium. Then I will talk about the research done at LPL in Quantum Dipolar Gas (QDG) team.

## 1.1 Chromium

Chromium is not an alkali, like most of the atoms in BEC experiments, it is situated on the $6^{th}$ column of the periodic table and therefore should have more than one valence electron. Actually, the electronic structure of Chromium is an exception to the standard filling rules: the 3d subshell is only half full and there is one electron is the subshell 4s ($[Ar]3d^5 4s^1$). Chromium therefore has 6 valence electrons and its spin is S = 3. One may ask the point of having 6 electrons, since the physics of atoms with 1 electron is already complicated enough. The answer is that with 6 electrons, the magnetic Dipole Dipole Interactions (DDI) are no longer negligible. Indeed, the dipole of an atom presents a magnetic moment proportional to its spin $\vec{\mu} = g_S \mu_B \vec{S}$ (with $g_S$ the Landé factor, $\mu_B$ Bohr's magneton, and $\vec{S}$ is the spin angular momentum) which creates a magnetic field $\vec{B}$ who will exercise a force on the other dipoles. The interaction potential between two particles separated by $\vec{r}$ is:

$$V_{dd}(\vec{r}) = \frac{\mu_0 (g_S \mu_B)^2/(4\pi)}{r^5}\Big(r^2 \vec{S_1}.\vec{S_2} - 3(\vec{S_1}.\vec{r})(\vec{S_2}.\vec{r})\Big). \tag{1}$$

This expression explicitly contains the two main features of DDI. The interaction is anisotropic since it depends on the respective orientations of the moments $\vec{\mu_i}$ and $\vec{r}$. Figure 1 is a scheme illustrating the anisotropy.

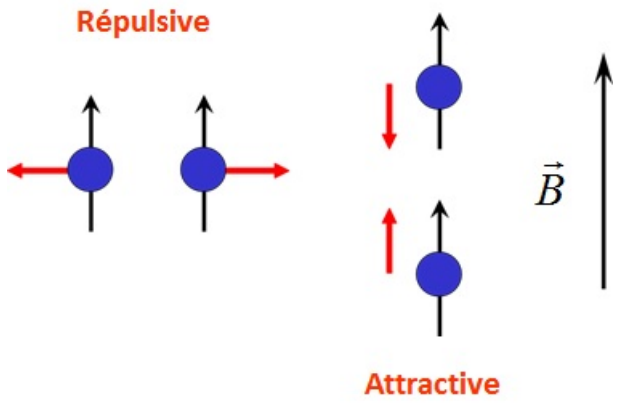


Figure 1: Scheme of Dipole Dipole Interactions. The interaction is repulsive for 2 atoms in a plane orthogonal to $\vec{B}$ and attractive if they are aligned along $\vec{B}$.

The other feature is that the potential is in $r^{-3}$, which is a long range potential.

DDI interactions are 36 times stronger than for an alkali, but it is still a weak interaction compared to the contact potential even for Chromium:

$$\epsilon_{dd} = \frac{V_{\text{dd}}}{V_{\text{Contact}}} \approx 0.159\ . \tag{2}$$

Though these interactions are weak, they are capable of coupling two atoms in different lattice sites (distance of a few hundred nm) and therefore lead to physics unattainable with alkali atoms.

## 1.2 Chromium at LPL

Laburthe *et al.* measured the effects of DDI thanks to the anisotropy of the interactions: for 2 orthogonal directions of the magnetic field, the interactions go from attractive to repulsive and modified the hydrodynamic properties of the condensate ([4],[5]). Then they turned their attention to magnetism, studying the low temperature phase diagram including the spin degrees of freedom [6]. Finally they set up an optical lattice in which they charged the BEC and studied the dynamics of magnetization [7]. A BEC with DDI in a lattice is particularly interesting since the hamiltonian of such a system is analogous to the Heisenberg hamiltonian. The spin-spin interactions being modelled by the long range DDIs. Therefore by studying the results of the dynamics of the system, we have access to the N-body Heisenberg problem. It is therefore possible to investigate such many-body problems related to quantum magnetism, which is particularly interesting as these problems are theoretically intractable due to many particle correlations.

The goal of my internship is to produce an optical dipole trap of specific size ($40\mu m$ horizontally and $10\mu m$ vertically). These trapping dimensions will create a 2D electron gas. The study of such a system is very interesting since new features which significantly modify the behaviour of the system. Our gaz is predicted to have spin domains and a 2D system will ease it's observation. The second part of my internship is to produce a non destructive spin sensitive *in situ* imaging system. Such an imaging system will be necessary to observe the spin domains. Future work will install lattices on the 2D gas. We will then be in the conditions of the Heisenberg hamiltonian and we will be able to observe spin dynamics of our system.

In the next part I will introduce optical dipole traps and give the characteristics of our trap with a beam waist of $40\mu$m horizontally and $10\mu$m vertically. In section 3 I will discuss the different characteristics of our imaging system.

# 2 Optical dipole traps

To be able to manipulate atoms a practical tool is light. Laser light can produce optical potentials up to a few mK. These Depths are just above typical Doppler temperatures, the limit temperature obtained by Doppler cooling, which range from 100$\mu$K to mK. Optical traps can be used on laser cooled atoms and we can proceed to evaporative cooling [8] to obtain BEC.

In this section I will introduce the concepts of atom trapping with an optical dipole trap, through a classical model which will enable us to introduce the polarisability. I will then give a quantum approach . For a thorough study of dipole trapping theory one should refer to [9]. Finally I will present the different characteristics of our trap.

## 2.1 Classical model

When an atom is illuminated by laser light, the electric field $\vec{E}$ induces an atomic dipole moment $\vec{d}$ which oscillates at the driving frequency $\omega$ of the laser. The amplitude $d$ of the dipole moment is related to the field amplitude by

$$d = \alpha(\omega)E \tag{3}$$

where $\alpha$ is the complex polarizability. The physical sense behind the polarizability is straightforward from this expression: it is the aptitude of an atom to align its dipole moment with the electric field.

In order to establish an expression for the polarisability $\alpha$, we will consider the atom in Lorentz's model of a classical oscillator. Lorentz thought of the atom as a nucleus connected to the electron (of mass $m_e$ and electric charge $e$) by a spring. The spring would be set into motion by an electric field interacting with the charge of the electron by either repelling or attracting the electron which results in either compressing or stretching the spring. The oscillation eigenfrequency $\omega_0$ corresponds to the optical transition frequency. Damping results from the dipole radiation of the oscillating electron. The equation of motion of the electron is

$$m_e\ddot{\vec{r}} + m_e\Gamma_\omega\dot{\vec{r}} + m_e\omega_0^2\vec{r} = -e\vec{E} \tag{4}$$

where $\Gamma_\omega$ is given by the power radiated by an accelerated charge [10]. This equation yields

$$\vec{r} = -\frac{e}{m_e(\omega_0^2 - \omega^2 - i\omega\Gamma_{\omega)}}\vec{E}. \tag{5}$$

Using equation (3) and the definition of the dipole moment of an electron $\vec{d} = -e\vec{r}$, we find the following expression for the polarisability:

$$\alpha = 6\pi\epsilon_0 c^3 \frac{\Gamma/\omega_0^2}{\omega_0^2 - \omega^2 - i(\omega^3/\omega_0^2)\Gamma} \tag{6}$$

where $\Gamma = (\frac{\omega_0}{\omega})^2\Gamma_\omega$ is the on-resonnance damping rate, and corresponds to the spontaneous decay rate for the resonant transition. The expression of the polarisability presented here is only valid for a 2 level atom, which is rarely the case. Nevertheless, this expression gives a good approximation and makes us understand the important quantities at stake for dipole trapping. The energy $U_{dip}$ of a dipole in an electric field is $-<\vec{d}.\vec{E}>$ and the power it radiates given by $\frac{dU_{dip}}{dt}$. For large detunings $\Delta = \omega - \omega_0$ one can express the interaction potential and the scattering rate:

$$\begin{aligned} U_{\text{dip}} &\propto \text{Re}(\alpha)I(r) \propto \frac{\Gamma}{\Delta}I(r) \\ \Gamma_{Sc}(r) &\propto \text{Im}(\alpha)I(r) \propto \left(\frac{\Gamma}{\Delta}\right)^2 I(r) \end{aligned} \tag{7}$$

Through these expressions, one can grasp the main properties of dipole trapping. One is there are two different types of dipole traps depending on the sign of the detuning $\Delta$. We can have a negative detuning ($\Delta < 0$) or a positive detuning. Negative detuning, or more commonly called "red" detuning, is when the driving frequency is below the atomic optical transition. In this case the dipole potential is negative and the potential minima are found at positions where the intensity is maximum. The interaction therefore attracts atoms into the light field. Positive detuning ($\Delta > 0$), or "blue" detuning, have a positive dipole potential and potential minima are found at positions of minimum intensity: the dipole interactions repels atoms from the light field.

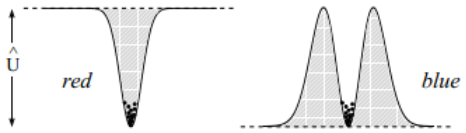


Figure 2: Illustrations of red-detuned traps and blue detuned traps. In the first case a Gaussian beam is illustrated and in the second a Laguerre-Gaussian $LG_{01}$ mode. Figure taken from [9].

The other feature is that the dipole potential scales with $\frac{I}{\Delta}$ whereas the scattering rate scales with $\frac{I}{\Delta^2}$. If a photon scatters it induces heating. We want the scattering rate to be as low as possible for a given potential depth therefore we use large detunings $\Delta$.

In our experiment we used a red-detuned dipole trap because it was the most adapted to our experiment. Also we are at very large detuning, indeed we want to trap atoms with light at $\lambda_{\text{Trap}} = 532\text{nm}$, and the optical transition for the $S_3$ to $P_4$ transition is $\lambda_0 = 425\text{nm}$. Our detuning is typically $\Delta \sim 10^{14}$, therefore we consider the scattering rate as completely negligible.

## 2.2 Quantum mechanical approach

The Lorentz model presented here is a very insightful method since it is very simple and allows to grasps the main concepts of dipole trapping. Its main limitation is that it can only describe with precision a 2 level atom. This is not the case for our system since the different Zeeman levels are very close to one another, and therefore we will trap atoms of different Zeeman levels. A multi atom level is necessary.

The interaction between an atom and the laser field can be treated in the dipole approximation since $\lambda_{\text{Trap}}$ is much larger than the size of an atom. The interaction can therefore be written under the following form

$$H' = -\mathbf{d}.\mathcal{E} \tag{8}$$

where $\mathcal{E}$ is the electric field

With second order perturbation theory, one finds [14] the energy shift for the ground state of an atom

$$\Delta E_g = -\frac{1}{2}\underbrace{Re\Big(\sum_e \frac{|<e|\mathbf{d}.\epsilon|g>|^2}{E_e - E_g - \hbar\omega - i\hbar\Gamma/2}\Big)}_{\alpha(\omega)}\frac{I(\mathbf{r})}{\epsilon_0 c}. \tag{9}$$

The theoretical trap depth, corresponding to the maximum value of $|\Delta E_g|$, is of $58\mu$K with our trapping conditions under 1 Watt of power, with a waist of $40\mu$m horizontally and $10\mu$m vertically.

## 2.3 Focused beam trap

In this section I will present you how we create a trap by a focusing a beam on the atoms, and explain the different characteristics of the dipole trap: shape, atomic density profile, trapping frequencies.

There are three main types of red-detuned dipole traps. Focused beam traps where one single beam is focused, and since the dipole force points towards increasing intensity it forms a trap. Standing wave traps, atoms are axially confined in the antinodes of a standing wave. And crossed beam traps, created by intersecting focused beam. A schematic of these traps are shown figure 3.


Figure 3: Schematic of the different types of dipole traps. (a) Horizontal focused beam trap, (b) Vertical standing wave trap, (c) Crossed beam trap. Image from [9].

We used the focused beam trap to produce the cigar shape form because it is the simplest and most adapted to our experiment.

The spatial intensity distribution of a Gaussian beam of power $P$ propagating along the z-axis is

$$I(x,y,z) = \frac{2P}{\pi w_x(z) w_y(z)} \exp(-2(\frac{x^2}{w_x(z)^2} + \frac{y^2}{w_y(z)^2})) \tag{10}$$

where $z$ is the axial coordinate and $w_x(z)$ (resp. $w_y(z)$ ) is the $1/e^2$ radius of the beam in the x-direction (resp. y-direction) and has the following form

$$w(z) = w_0 \sqrt{1 + (\frac{z}{z_\mathrm{R}})^2}. \tag{11}$$

$w_0$ is called the beam waist and corresponds to the minimum radius of the beam, $z_R$ is the Rayleigh length and is given by $z_\mathrm{R} = \pi w_0^2/\lambda$. The dimensions of our planned cigar shape beam are $\mathrm{w_x} = 40\mu$m and $\mathrm{w_y} = 10\mu$m which gives us a Rayleigh length of 1.18cm along the x-axis and $740\mu$m along the y-axis.

If the thermal energy $k_\mathrm{B}T$ of the atomic system is much smaller than the traps depth $|U(r=0,z=0)| = \hat{U}$, the extension of the atomic system is much smaller in the radial direction than the waist, and much smaller in the axial direction compared to Rayleigh length (figure 4). We can therefore approximate the dipole potential

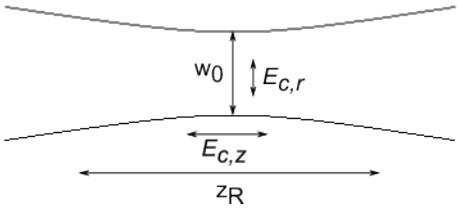


Figure 4: Scheme of a Gaussian beam where the axial extension is compared to the Rayleigh length and the radial extension to the beam's waist.

by a harmonic oscillator and it yields:

$$U(r,z) \approx -\hat{U}\left[1 - 2(\frac{x}{w_x})^2 - 2(\frac{y}{w_y})^2 - \frac{1}{2}(\frac{z}{z_{Rx}})^2 - \frac{1}{2}(\frac{z}{z_{Ry}})^2\right] \tag{12}$$

From this form of the potential, we can deduce the axial trapping frequency $\omega_z$ and the trapping frequencies $\omega_x$ and $\omega_y$ at the beam's waist.

$$\begin{aligned} \omega_\mathrm{x} &= \sqrt{4\hat{U}/mw_x^2} \\ \omega_\mathrm{y} &= \sqrt{4\hat{U}/mw_y^2} \\ \omega_\mathrm{z} &= \sqrt{\hat{U}/mz_R^2} \end{aligned} \tag{13}$$

with $\frac{1}{z_R^2} = \frac{1}{z_{Rx}^2} + \frac{1}{z_{Ry}^2}$

With our trap shape, and the value of the energy calculated in section 2.2 by the multi-level theory, we have the following theoretical trapping frequencies:

$$\begin{aligned} \omega_\mathrm{x} &= 750 \times 2\pi \text{ Hz} \\ \omega_\mathrm{y} &= 3 \times 2\pi \text{ kHz} \\ \omega_\mathrm{z} &= 25 \times 2\pi \text{ Hz} \end{aligned} \tag{14}$$

The values of these trapping frequencies seem logical since we find a strong trapping frequency vertically, and very loose horizontally. One worry is that since it is so loose, it could be sensitive to gravity or to a gradient of magnetic field even though they are compensated by magnetic fields.

## 2.4 Atomic Density Profile

Now that the shape of the trap is completely known, we must understand the atoms position distribution. In the following section we will derive the form of the atomic density $n(x, y, z)$ and find it has an inverse parabola shape.

The atomic ground state of a bosonic quantum system is given by the Gross-Pitaevski equation [11]:

$$\underbrace{-\frac{\hbar^2}{2m}\Delta}_{\text{kinetic term}}\ \psi + \underbrace{(V_{\text{Trap}} + g \times n(x,y,z) + \Phi_{dd})}_{\text{Potential term}}\psi = \mu\psi \tag{15}$$

where $n(x, y, z)$ is the density profile,$\Phi_{dd}$ is the dipolar contribution to the mean field interaction [12], and the term $g = 4\pi\hbar^2 a/m$ corresponds to a pseudo potential representing the contact interaction with $a$ the scattering length. Pethick and Smith performs a full calculation of the density profile of a Chromium condensate with dipole-dipole interactions and concludes that they only modify the size by a few percent [13].

In the x and z directions, the kinetic term is much smaller than the contact potential term therefore we say we are in the Thomas-Fermi regime. This approximation consists in neglecting the kinetic term in front of the contact potential term. In these directions, we therefore have an inverse parabola density distribution. In the y direction, it is the kinetic energy term which dominates in front of contact potential term. Therefore the equation reduces to the equation of harmonic oscillator, with the solution a Gaussian function. Because this is an approximation, it is not completely Gaussian. We therefore have the following density profile

$$n(\mathbf{x},\mathbf{y},\mathbf{z}) = n_0\big[1 - (\frac{x}{R_x})^2 - (\frac{z}{R_z})^2\big]e^{\frac{-m\omega_y^2 y^2}{\hbar}} \tag{16}$$

where $n_0 = \frac{\mu}{g\sqrt{2}}$ is the peak density with $\mu$ the chemical potential and

$$\begin{aligned} R_x &= \sqrt{\frac{2\mu}{mw_x^2}} \\ R_z &= \sqrt{\frac{2\mu}{mw_z^2}} \\ a_y &= \sqrt{\frac{\hbar}{mw_y}} \end{aligned} \tag{17}$$

are the Thomas-Fermi radii in the x-direction (resp. z) and the oscillator length in the y-direction. As one can see, the chemical potential is a key parameter in the physics of BEC since it sets the peak density and the size of the condensate. It also dictates when condensation takes place. Indeed it is defined as the energy you need to bring to the system to add a particle and for the system to keep it. If we had a non interacting BEC, it doesn't cost any energy to bring a particle in the fundamental state so $\mu = 0$. For a system with interactions in 3D, the chemical potential is worth the interaction energy $\mu = \text{gn}$. The chemical potential for a 2 dimensional gas is defined by:

$$\mu = \frac{\hbar\omega_y}{2} + \frac{g}{\sqrt{2}}n_{2D}. \tag{18}$$

with $n_{2D}$ the two dimensional density. In our trap we have typically 15000 atoms which yields:

$$\mu = h \times 4.5\text{kHz} \tag{19}$$

$$n_0 = 1.810^{20}\text{at.m}^{-3} \tag{20}$$

$$\begin{aligned} R_x &= 1.3\mu m \\ R_y &= 430nm \\ R_z &= 116\mu m \end{aligned} \tag{21}$$

The theoretical size of the condensate is as desired. Though, for our system to be described as 2D gas, we need $gn_{2D}/\sqrt{2} >> \mu/\hbar$ which is not the case. We therefore have a gas that is not 2D, but nearly. It is very hard to produce a purely 2D gas and to obtain a condensate with these typical dimensions would be very satisfying. An easy way of producing a 2D gas is with lattices where typical oscillation frequencies is of the order of 50kHz. Unfortunately it is not possible to isolate one lattice site from the others.

## 2.5 Experimental Results

After choosing the specific optics to produce a beam with the desired waist, we aligned the beam on the BEC. The atoms were not as confined as one as expected. We therefore measured the y-axis trapping frequency (figure 5). The principle of the measurement is the following: the atoms are in the trap, the trap is suddenly

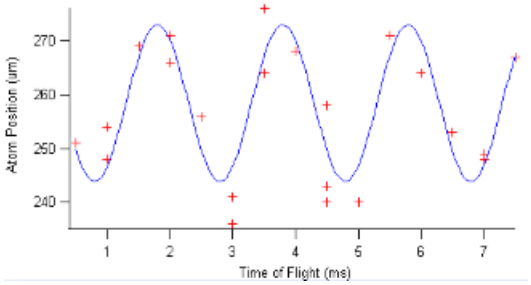


Figure 5: Measurement of the trapping frequency along the vertical axis. The trap is turned off and back on, making the atoms oscillate. The atoms' position was probed after different times. By fitting with a cosine function, we find a trapping frequency of 500 Hz, which is one order of magnitude smaller than expected. The difference is explained by the beam not having the correct sizes.

turned off and back on, we then measure the position of the oscillating atoms after different times. We measured a trapping frequency of 500Hz which is 6 times too small.

We then imaged the beam and noticed that it wasn't at all at the correct sizes, the focus point wasn't the same for both axis and it had an ugly shape. We corrected those points (the ugly shape was caused by one of the cylindrical lenses'), characterized the beam along the optical path, and produced a beam of the desired waist: 40$\mu$m horizontally and 11$\mu$m vertically (figure 6).

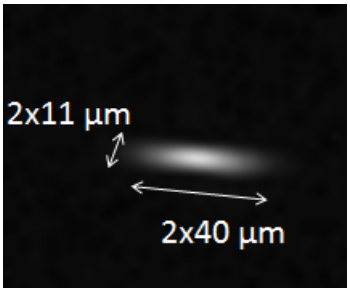


Figure 6: Image of the beam at the focal point after corrections. The astigmatism and size were corrected by replacing the lenses. The parasite light disappeared when we changed the cylindrical lens with a cylindrical lens with a better anti reflect treatment. The beam has an horizontal waist of 40$\mu$m and a vertical waist of 11$\mu$m

We then proceeded to aligning the beam back on the BEC and measured the trapping frequency using parametric oscillations. This method consists in modulating the intensity of the trapping beam at a certain frequency. This modulation only induces heating in the trap if the modulation frequency is twice the trapping frequency [23]. Figure 7 shows the temperature as a function of the modulation frequency. The measured trapping frequencies are:

$$\begin{aligned} \omega_x &= 800 \times 2\pi \text{ Hz} \\ \omega_y &= 2.4 \times 2\pi \text{ kHz} \\ \omega_z &= 15 \times 2\pi \text{ Hz}. \end{aligned} \tag{22}$$

These results need to be corrected by the transfer function of the Acoustic Optic Modulator. Indeed the AOM has not the same efficiency in function of the input voltage. This transfer function has yet been measured but we expect it to change little the result because a measurement of the collective excitation yields a trapping frequency in the y-direction of 2.5 kHz and this experiment is independent of the AOMs transfer function. We therefore produced a gas in very good agreement with expectations.

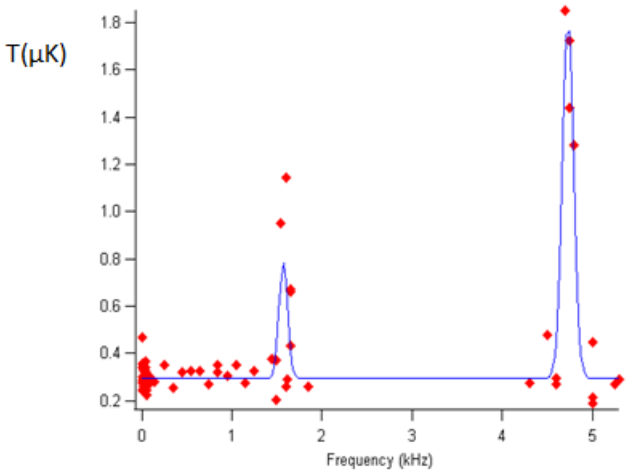


Figure 7: Measurement of the trapping frequencies through the method of parametric oscillations. Heating in the trap is induced when the modulation frequency of the trapping light is equal to twice the trapping frequency. Each peak corresponds to twice the trapping frequency. The measured trapping frequencies are 800 Hz in the x-direction, 2.4 kHz in the y-direction, and 15 Hz in the z-direction.

# 3 Imaging a BEC

During my internship, we also started setting up a new imaging system. The goal of this imaging system is to image *in situ* the spin states of atoms in new dipole trap. The physical idea behind measuring spin states is that the interaction of light in a given polarisation state is not the same given the spin state of the atom. In a first part, I shall describe the optic system which gives us a resolution of 2.5$\mu$m, and give its main characteristics. Then I shall introduce different BEC imaging system, briefly focusing on the prior imaging system which is an absorption image after expansion of the condensate (i.e. after time of flight), before presenting the new system.

**Mount Design**

The optical table is very crowded, and where the condensation takes place there are so many optics it makes the implementation of the imaging system extremely hard. Figure 8 is a picture of the table and shows the little space left.

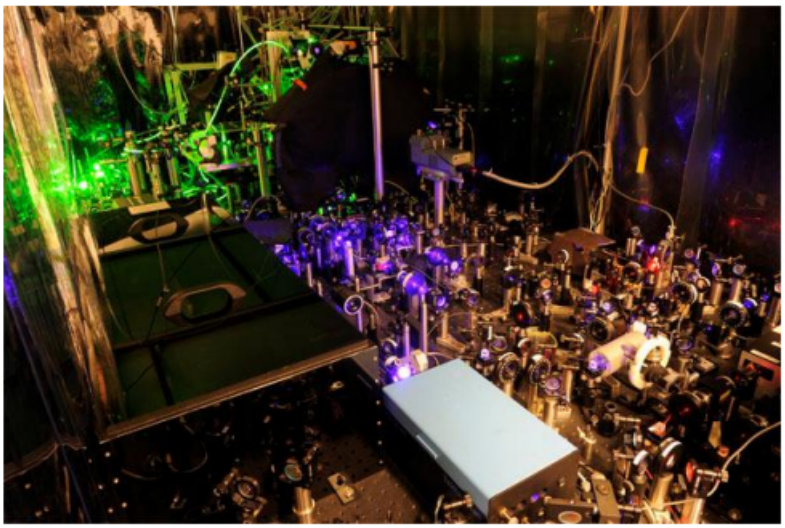

Figure 8: Picture of the optical table. Even though the BEC is at the far end of the table, the picture shows how crowded the table is and the difficulty of access we will have when we will set up the imaging system.

We would like to image the atoms through the vertical axis since our atoms are tightly confined in the horizontal plane. There is already the MOT beam on the vertical axis, therefore we have no choice but to image the atoms with a beam slightly tilted (by $7^\circ$) from the vertical axis. I designed a mount (figure 9) for the imaging system which has a specific size and angle and should help us in aligning the beam on the BEC.

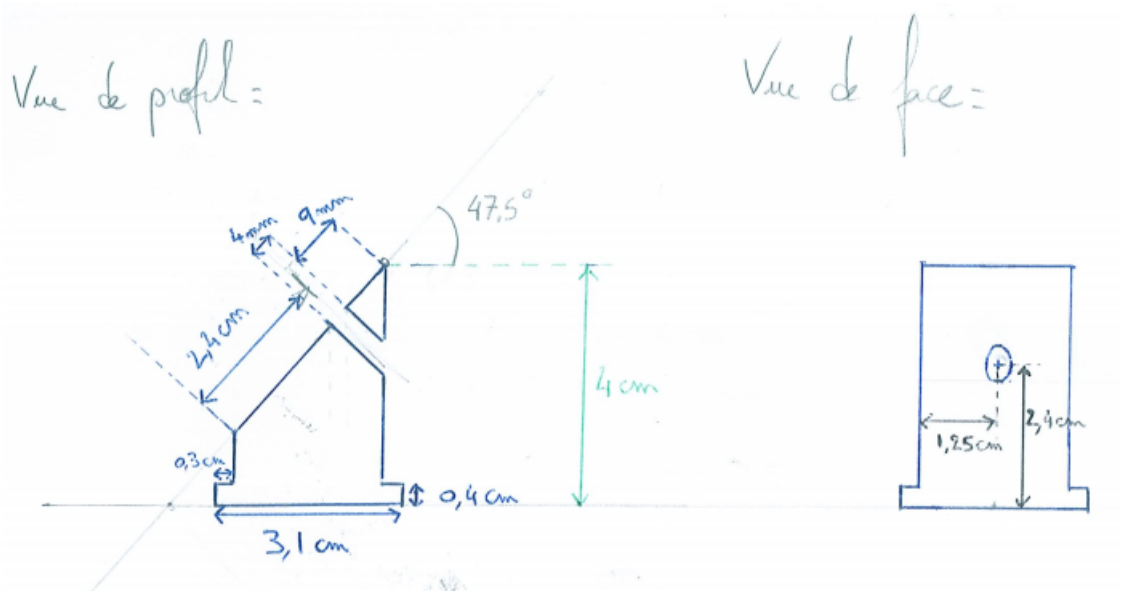


Figure 9: Scheme of an optical mount for the imaging system designed with specific size in order to make the optical path to the BEC a little easier.

## 3.1 Optical System

### 3.1.1 Resolution of an optical system

The resolution of an optical system is defined as the minimum distance between distinguishable objects in an image. The physical reason behind an optical system having a finite resolution is that a lens has a finite size. To understand the effect we will use the simple example of a beam with a Gaussian intensity distribution. A Gaussian distribution expands from infinity to infinity, even if it has a very small width. As the beam goes through the lens, the lens cuts the tails of the Gaussian distribution, as a result the beam will be diffracted and have a finite size. Through this we understand that the bigger the lens the better (i.e the lower) the resolution. Rayleigh calculated the intensity distribution of a point source object diffracted by a circular aperture, and defined the Rayleigh criterion as the resolution of a system:

$$\Delta l = 1.22\lambda \frac{f}{D} \tag{23}$$

with $\lambda$ the wavelength, $f$ the focal distance of a lens and $D$ its diameter. We would like a resolution of about $2\mu m$. We opted for using an achromatic doublet from Thorlabs of focal length $f = 200mm$ of aperture $D = 50.8mm$ which should allow us to have a maximum resolution of $\Delta l = 2.04\mu m$. The team had already used this lens before, and in A. Pouderous thesis [16] he explains how the lens was carefully chosen to minimise spherical aberrations.

### 3.1.2 The Optical System

The optical system cannot simply be a lens and a camera since the camera has big pixels of $14\mu m$. We need a minimum telescope of magnification 7 so that the resolution of the imaging is limited by the lens (i.e. limited by diffraction), and not the pixel size of the camera. We will use a 7.5 magnification telescope. Therefore the maximum resolution of the system is $\Delta l \times 7.5 = 15.3\mu m$ and we should not be limited by the pixel size but by the diffraction limit. Since the Thorlabs lens of $f = 200mm$ will be the first lens, and we need a magnification 7

telescope we have two options: or use a lens with a minimum focal length of 1400mm, or use an other f=200mm Thorlabs lens therefore building a 1 magnification telescope and then a 7 magnification telescope. We opted for the second solution since it was the most convenient for our experiment. The optical system to image is the following:

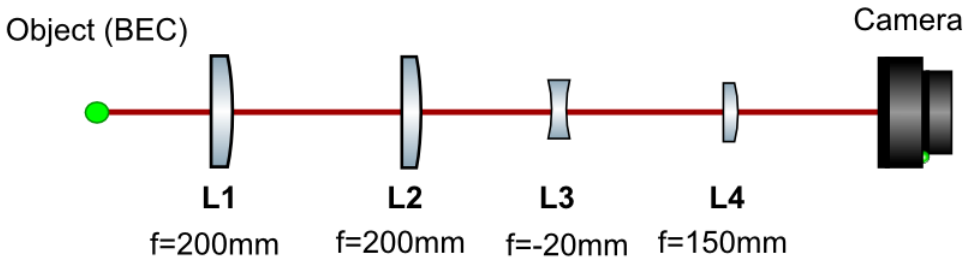


Figure 10: Optical system used to image a BEC. Lenses L3 and L4 form a 7.5 magnification telescope. L1 sets the diffraction limit of our system.[19]

The distance between each lens (the focal distance for the distance object-L1 and L4-Camera, the sum of the focal distance for the others) is justified by Gaussian optics in order to perform a relay system.

**Camera**

The camera used for the imaging system will be an Andor camera. This is a luxurious camera with high sensitivity for light at 400nm, with a quantum efficiency of about 0.9. It can be cooled down to -100 $^\circ$C, which is critical for elimination of dark current detection limit. It is a single photon sensitive camera which has an electron multiplier feature with less than a photon noise. I did not use this camera for the characterisation of the optical system but a Lumenera camera. The lumenera camera has not got as exceptional characteristics as the Andor, but it produces images with excellent sensitivity and low dark current.

**Determination of the resolution**

To measure the resolution of our system, we used a test target of Thorlabs. This target is a set rectangular bars of different known sizes (figure 11) and the resolution of the optical system is determined by the first set of undistinguishable bars.

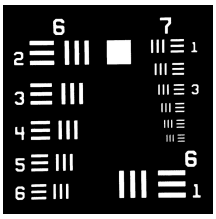


Figure 11: Image of the test Target. Each set of rectangular bars have different sizes, and the resolution of the optical system can be determined by the first set of bars that we cannot distinguish

The smallest set of bars is of 4.38$\mu$m, i.e. bigger than the resolution of our system. Therefore to evaluate quantitatively the resolution we used a more complete technique. The electric field distribution of a point source object diffracted by a circular aperture is the Airy function. Therefore for 3 source point it is the sum of 3 Airy functions and the intensity distribution should be given by (for a beam propagating along the z-axis):

$$I(r,z) = A\left|\frac{J_1(\frac{kD(r-a)}{2z})}{\frac{kD(r-a)}{2z}} + \frac{J_1(\frac{kDr}{2z})}{\frac{kDr}{2z}} + \frac{J_1(\frac{kD(r+a)}{2z})}{\frac{kD(r+a)}{2z}}\right|^2 \tag{24}$$

where $k$ is the wave vector, $A$ the amplitude, $z$ is the distance between the object and the lens, $D$ the lens aperture, and $a$ is the distance between the center of 2 rectangles. This form of the distribution is an approximation since the rectangles we are imaging are not point source objects. The correct distribution would be given by the squared modulus of the Fourier Transform of the convolution of the objects electric field distribution [18].

This is a heavy calculation (even for Mathematica!). We found that for a system which is diffraction limited the intensity distribution (24) is a very good approximation.

Fitting our data with (24) we have access to the effective diameter of the lens, and through (23) we have the resolution of our system, which we optimized to $2.5\mu m$. Figure 12 shows a picture of the USAF target with our imaging system, with a fit of the intensity profile giving us the effective diameter of the lens.

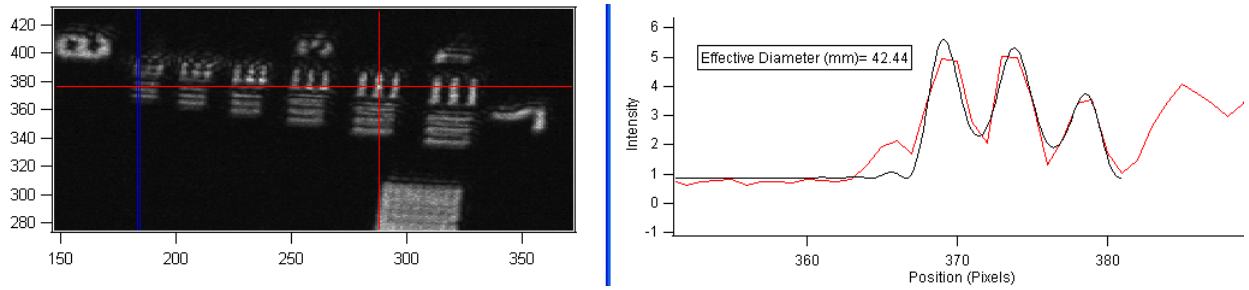


Figure 12: Picture of the USAF target. We can see a clear astigmatism between the two axis and there is no reason why one axis should be resolved better. By moving the camera by a few micrometres, we can give the other axis a better resolution. Fit of the intensity profile with (24) to determine the effective diameter of the lens. From that we can determine the resolution of the system.

It is very important for us to know if a lens's position is very sensitive to the resolution. Indeed if we find that a lens needs to be exactly at a certain position for the resolution to be optimized, we will have to be careful in placing it. In the next paragraph, we will study the importance of the position of each lens.

**Resolution dependence on the lens position**

One should place each optical element at the focal distance or the sum of the focal distance. But experimental factors make that it can differ slightly.

Since the two first lenses form a virtual object at the focal distance of the third lens, these 2 lenses play a "translational" role in the sense that the first lens (L1) is equivalent to the third (L3), and the second (L2) to the fourth (L4).

We can understand that the first lens is going to be the most important. Indeed, as light passes through the object, the smallest dimensions, corresponding to the largest frequencies get more diffracted, and therefore if the lens is too far it will not "catch" these frequencies. Here the lens plays the role of a frequency filter. One could think that we must place the lens just behind the object. If we do that, the small frequencies will be caught by the first lens, but not by the second since the beam wouldn't be collimated. Figure 13 shows the resolution of the system by changing just the distance between the lens and the object.

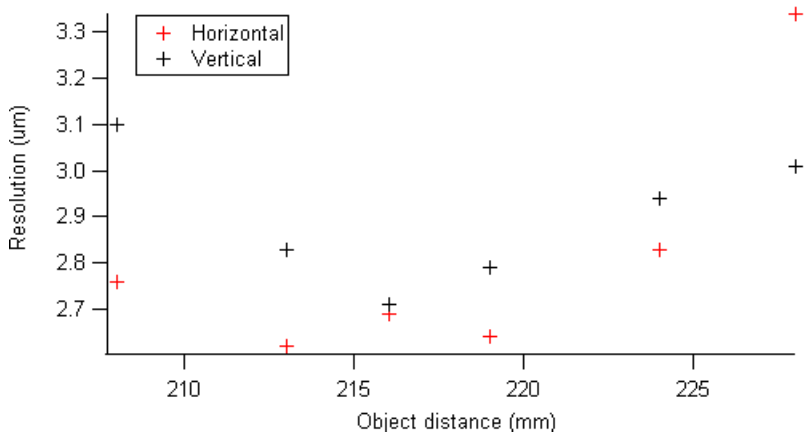


Figure 13: Horizontal and vertical resolution of the optical system as a function of the distance between the first lens and the object. The data suggests we need to be precise at the mm to minimise the resolution

The data, confirmed by predictions made with Zemax, suggests that the position of the lens must be placed at the millimetre scale in order to minimize the resolution and that it must placed at 215 mm from the object. We will therefore place the lens on a translational mount. These mounts allow us to place an object with a precision of 10$\mu$m. It is quite surprising to find that the best resolution is found so far away from the focal distance. We believe the reason is the lens is slightly further it catches a little less the big frequencies but suffers less from aberrations. Therefore the theoretical resolution of the lens placed 21.5cm is slightly worsened ($\Delta l = 2.2\mu$m) but the experimental resolution is better.

At the exit of the first lens, the image is collimated and therefore we shouldn't lose much information. In fact it should only affect the transverse resolution, leaving the resolution on the optical system untouched. Changing the position of L4 over centimetres and measuring the system's resolution we concluded that it's position is not critical for the resolution on axis. (figure 14). Its position should however affect the transverse resolution so it will still be placed carefully, so that the distance between L1 and L2 is $f_1 + f_2$.

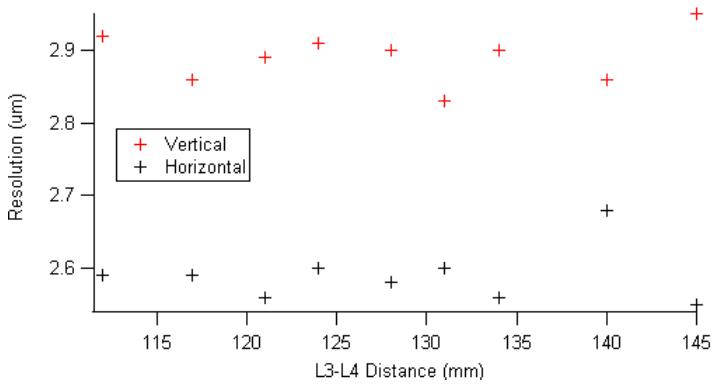


Figure 14: Horizontal and vertical resolution of the optical system as a function of the distance between the third and fourth lens. The data suggests that we do not need to be very precise on the position of the fourth lens.

The third lens is the same lens as the first one exept that its even more sensitive. Indeed there is a factor 4 between their focal lengths so a mm precision becomes a 250$\mu$m precision, and therefore it is necessary to put a translational mount so that the image of the object through the 2 first lens is exactly at the right position.

The second lens plays the same role as the fourth and therefore doesn't affected the resolution on axis and we will not need a translational mount in order to place it.

Now that the resolution of our optical system along the optical axis is known, we must study the in-plane resolution (the transverse field resolution) i.e. study the resolution as we move away from the optical axis. It is important that it does not deteriorate too fast since we would like to ascertain spin population over the whole trap. By moving the object in it the object plane and evaluating our resolution, we find, in agreement with predictions made by Zemax, that the resolution does not deteriorate over a large distance (figure 15). We can conclude from the data that our experimental transverse field resolution is of at least 400$\mu$m since the resolution of the object 400$\mu$m off axis is as good as on the optical axis. This is an important result because we know that the resolution of our system will be the same over the entire condensate.

The depth of field of our system must be known. Experimentally we find that the resolution of our optical system not very sensitive on the position of the camera: the resolution did not change over a displacement of 1.5mm.

The atoms are in a metallic chamber with thick view ports. We placed an equivalent piece of glass in our setup, with a tilted angle, to simulate the experimental condition and the resolution is not destroyed (it changes by less than 10%). This is an important result because one could think that the angle could introduce aberrations to the system. Fortunately it did not and we obtain a resolution of about 2.9$\mu$m. Finally, we placed a piece of glass to simulate the effect of the phase spot glass (see section 3.3.2) on the resolution, which did not change the resolution.

The optical system has been completely characterized. We have a resolution of 2.9$\mu$m close to the limit of diffraction (2.2$\mu$m). The resolution doesn't get attenuated over the typical size of our trap. The depth of field is large, of at least 1.5mm. The effect on the resolution of each lens has been evaluated, the second and fourth lens's position are not critical but the first and third ones are that's why we will use a translational mount to

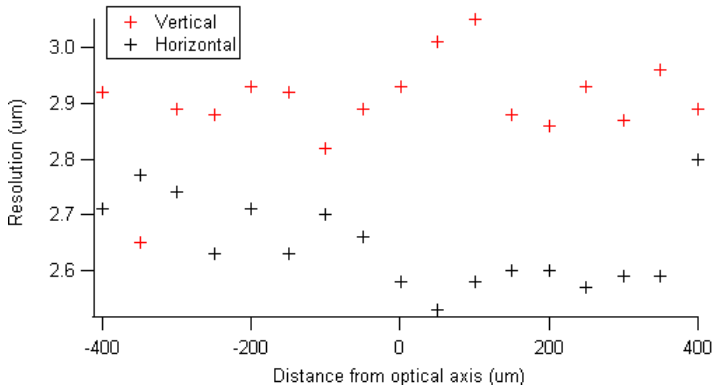


Figure 15: Horizontal and vertical resolution of the optical system as a function of the distance to the optical axis. From the data we can conclude that our transverse field resolution is of 800$\mu$m

place them. Finally, to put ourselves as close as possible to experimental conditions we placed a piece of glass. The glass was used to simulate the glass cell and the phase spot. We concluded that they will not destroy the imaging resolution of our setup.

## 3.2 BEC imaging systems

There are two main types of imaging system, in-situ and time of flight imaging. In both cases we image the column density distribution of atoms, but either with the atoms in the trap or after a ballistic expansion. These techniques can be used either by shining resonant light which the atoms will absorb and hence destroys the condensate. Or by shining non resonant light, which the atoms don't absorb but de-phase. The new imaging system relies on the latter principle. Whereas the prior imaging technique, a Stern and Gerlach analysis, is absorption imaging after time of flight. This analysis allows us to ascertain the populations of the different Zeeman sublevels and works the following way. A magnetic gradient is pulsed upon the condensate while it is in expansion. This pulse results in a spatial separation of each spin state since the strength of the interaction between magnetic field and an atom depends on the spin state of the atom ($\mathrm{E} = \mathrm{m_s g} \mu_\mathrm{B} \mathrm{B}$, where $m_s$ is the spin state $\mu_B$ Bohr's magneton and $g$ the Lande factor, and $\mathbf{F} = -\nabla E$). This type of imaging is called Stern and Gerlach analysis in reference to Stern and Gerlach experiment in which atomic spin was demonstrated [20]. Figure 16 is a typical image of the prior imaging technique. The spatial separation induced by the magnetic pulse allows us to clearly identify the population of each spin state.


Figure 16: Image from the prior imaging technique: Stern and Gerlach analysis of a Chromium BEC. The different spin states are separated by a magnetic pulse and then imaged after a time of flight. Since Chromium has $\mathrm{S} = 3$, there are 7 Zeeman sub-levels. The intensity of the spot is related to the population, therefore the spin state $\mathrm{m_S} = -3$ has a larger population than the other spin states. Image taken from [17]

## 3.3 Non destructive in situ imaging system

The prior imaging technique was very instructive since it allows precise measurement of the population of each spin state. But it has two main limitations which motivates us to install the new system. First, it is a measurement after expansion of the condensate, therefore we cannot see the spin dynamics inside the trap. In particular, the visualization of spin domains is not possible. And secondly, absorption imaging only allows us to measure the population of each state, but not the coherences between each spin state. Through phase imaging one can probe coherences and this could be an interesting development to the imaging system I present here.

### 3.3.1 Phase Contrast Imaging

The method of phase contrast imaging was invented by Zernike in the 1930s [21]. The method consists in interfering a light that underwent a phase shifted with unshifted light (like all phase measurement techniques). Where our method differs from an ordinary interference measurement is by phase shifting the non diffracted light by inserting a small object (i.e something with a refractive index different from 1) called a phase spot. Figure 17 shows a scheme to illustrate the method.

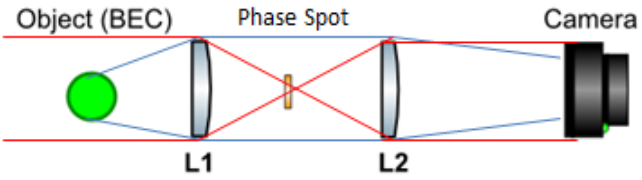


Figure 17: Scheme of Phase Contrast Imaging method. The unscattered part of the beam (part of the beam that doesn't go through the BEC) focuses on the phase spot (See section 3.3.2) and gets phase shifted. The scattered part is barely affected by it, but is phase shifted by the BEC.

The phase spot will introduce a phase $\theta$. The electric field in the image plane can be written as:

$$E = E_{\text{Unscat}} e^{i\theta} + E_{\text{Scat}} \tag{25}$$

The complex phase accumulated by the scattered light in a medium is $\phi_{atoms} = \phi' + i\phi$" where $\phi'$ is the phase shift and $\phi$" is the optical density. To isolate locally phase shifted photons, formally this is equivalent to making the difference between a beam which locally phase shifted and a beam which is not phase shifted. Hence the electric field is

$$E = E_{\text{Unscat}} e^{i\theta} + E_{Unscat}(e^{i\phi_{\text{atoms}}} - 1) \tag{26}$$

and the intensity distribution is given by

$$I = I_0(2 + e^{-2\phi"} - 2\cos(\theta) + 2\cos(\theta - \phi') - 2\cos(\phi')e^{-\phi"}). \tag{27}$$

From this expression, the importance of the phase spot is clear. If there were no phase spot, $\theta = 0$, the intensity no longer depends on $\phi'$ because the terms cancels themselves out. On the other hand, with a phase spot chosen such that $\theta = \frac{\pi}{2}$, and $\phi_{atoms} << 1$, there is a linear dependence on the phase shift created by the atoms:

$$I = I_0(1 + 2\phi') \tag{28}$$

We have just established the relation between the intensity signal we will measure, to the phase caused by the atoms. Since we would like to perform non destructive imaging, we hope to keep $\phi$" close to 0 in order to have the least absorption possible. In the following I will start by presenting the characteristics of the phase spot we produced, then I shall show how to relate this phase shift to the atomic density profile calculated in 2.4, and finally to the atomic spin state.

### 3.3.2 Characterisation of the phase spot

In order to build the phase spot, I worked in collaboration with Thierry Billeton of the optic workshop. We deposited by evaporation $300nm$ of $MgF_2$ of $200\mu m$ wide on the glass. We wanted $280nm$ since, knowing the refractive index of $MgF_2$, it would create the $\frac{\pi}{2}$ phase shift desired. The $200\mu m$ width was decided from a competition between being big enough to be able to align the unscattered light on the spot (the unscattered beam should have a size of about $10\mu m$), but not too big that it would dephase too much the scattered beam. We measured the spot sizes in a clean room with a profilmetre and found $300nm$ height and $250\mu m$ wide. The sample measured was only a test, and the final evaporation was produced in the same conditions. We will only characterise it optically in order to not damage it ( more exposure to dust, mechanical pressure during measurement, ...) and to determine the phase shift it creates.

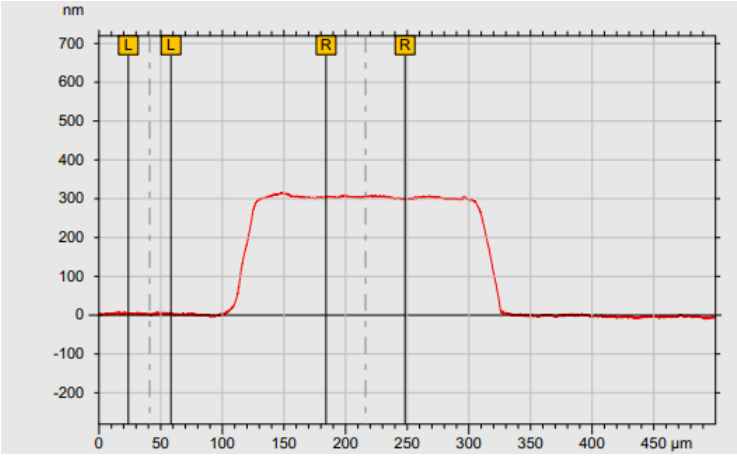


Figure 18: Characterisation of the phase spot size (height and width) with a profilmetre. We measured $300nm$ height and $250\mu m$ of width. Such a spot should able us to dephase the unscattered beam by $\frac{\pi}{2}$.

### 3.3.3 Refractive index of a cold atom gas

It is clear that the phase shift created by the atoms is linked to its refractive index $\mathcal{N}$. There are two main physical quantities on which the refractive index depends on the atomic density $n$ of course but also and mainly on the atomic polarisability $\alpha$. Indeed the phase shift is caused by the modification of the polarisation of the probe field by the atomic dipoles. Since we hope to observe spin domains, it is the difference of polarisability of each spin state which is going to make this possible. The expression of the refractive index is

$$\begin{aligned} \mathcal{N}^2 &= 1 + n\alpha \\ \Rightarrow \mathcal{N} &\approx 1 + \frac{1}{2}n\alpha \end{aligned} \tag{29}$$

Light passing through a medium with an index of refraction $\mathcal{N}$ over a distance $L$ accumulates a phase $\phi_{\text{atoms}}$:

$$\phi_{atoms} = k_{\text{image}}(\mathcal{N} - 1)L \tag{30}$$

where $k_{\text{image}}$ is the imaging light wavenumber. Since the atomic density depends on the position, the phase shift also depends on the position and we have for an imaging light in the y direction:

$$\phi_{atoms}(x,z) = k_{\text{image}}\frac{\alpha}{2}\underbrace{\int_{-R_y}^{R_y} n(x,y,z)dy}_{\text{Column density } = \text{ n}_\text{c}}. \tag{31}$$

As discussed in section 3, we will not image the atoms along the y-direction since the MOT beam is already occupying it. We are imaging with a tilted angle of $7^\circ$ and therefore we must integrate along that axis, which implies a simple variable change for the integral in 31. Since the intensity of light after passing through a medium is $\mathrm{I} = \mathrm{I}_0 \mathrm{e}^{\mathrm{i}\phi_{\text{atoms}}(\mathrm{x,z})}$, the real part of $\phi_{\text{atoms}}$ (proportional to $\mathrm{Re}(\alpha)$) is proportional to the phase shift. And the imaginary part of $\Phi$ (proportional to $\mathrm{Im}(\alpha)$) to the absorption.

For simplicity, we will use the expression of $\alpha$ obtained for a 2-level atoms (equation (6)). This expression is however incomplete since it considers only the electronic orbital wavefunctions (related to the spontaneous decay rate $\Gamma$), and didn't take into account the coupling between the laser polarisation and the electronic and nuclear angular momenta involved. More precisely in section 2, we assumed only the coupling between electronic orbital function of different states:

$$|<i|d|j>|^2 = \frac{3\pi\epsilon_0\hbar c^3}{\omega_0^3}\Gamma. \tag{32}$$

Taking into account the electronic and nuclear angular momenta and the laser polarisation this expression becomes:

$$|<i|d|j>|^2 = \frac{3\pi\epsilon_0\hbar c^3}{\omega_0^3}\Gamma \times c_{ij}^2 \tag{33}$$

where $c_{ij}$ is the Clebsch-Gordan coefficient of the considered transition. The different Clebsch-Gordan coefficients can be found in Appendix.

### 3.3.4 Experimental Issue

In the experiment, imaging the atoms will consist in taking three images. The first image, taken with atoms in the trap and the imaging light, yields $\mathrm{I_{atoms}(x,z)}$. The second image contains the intensity of the imaging light $\mathrm{I_0}$. This image is necessary since it allows us to know the intensity profile of the unscattered part of the imaging beam. The third image is the intensity profile of the background, with no light nor atoms. We take this picture to subtract the contribution of the background of each image and to only have the atomic contribution. The normalized intensity profile of the atom is given by:

$$I(x,z) = \frac{I_{\text{atoms}} - I_{\text{background}}}{I_0 - I_{\text{background}}} \tag{34}$$

Using equation (28), we can relate our image information to the atomic phase.

### 3.3.5 Theoretical Results

In this section I will show plots using the theory developed in 3.3.1 and in 3.3.3. In the following figure (figure 19), I plot the expected measurements. There is only little dephasing since the imaging beam only see few atoms (we image along the most confining axis), therefore to have a measurable dephasing we have to choose a light frequency very close to resonance. But as we get closer to resonance the atoms will absorb light more and more and the measurement will be destructive. These graphs are performed for a detunning $\Delta = 5\Gamma$ and are 1D plots over the condensate along the trapping beam axis. The top left graph shows typical dephasing and the top right the absorbance. We have a dephasing of 0.2 rad and an absorbance 0.005 which shouldn't be too destructive. In the bottom plot, I supposed that the atoms situated from $-\mathrm{R_z}$ to 0 were in the spin state $m_S = -3$ and the ones from 0 to $\mathrm{R_z}$ were in the spin state $m_S = -2$ and plotted the phase profile and normalized intensity profile. We see that the difference of dephasing is of 0.1. To know if we can measure this signal, we need the noise of the camera $\beta$ to be smaller than the difference we should measure:$\beta < 0.1 \times I$. The noise of the camera is inferior to 1 in the electron multiplier mode. Therefore we should be able to measure the spin state of the atoms. The extreme sensitivity of our camera will allow us to shine minimum power on the atoms to have minimum absorption, i.e. minimum heating, but our imaging system will not be completely non destructive. To be non destructive, the number of atoms must be greater than the number of atoms absorbing a photon:

$$\begin{aligned} N_{\text{Abs}} &<< N_{\text{At}} \\ \rightarrow \frac{\Delta I \times S}{\hbar\omega} t &<< N_{\text{At}} \\ \Rightarrow t &<< \frac{n_c \times \hbar\omega}{0.005 I_0} \end{aligned} \tag{35}$$

with $n_c$ the column density, and $I_0$ the intensity of the imaging light. For a light intensity comparable to the saturation intensity (about $10\mathrm{mW.cm^{-2}}$), this condition implies image pulses shorter than a few microseconds.

Due to the fact that the atomic density along the imaging axis is not very large, we need to image with light very close to resonance to create a significant dephasing. We should be able to implement a phase contrast imaging system to the experiment, unfortunately it will be a little destructive.

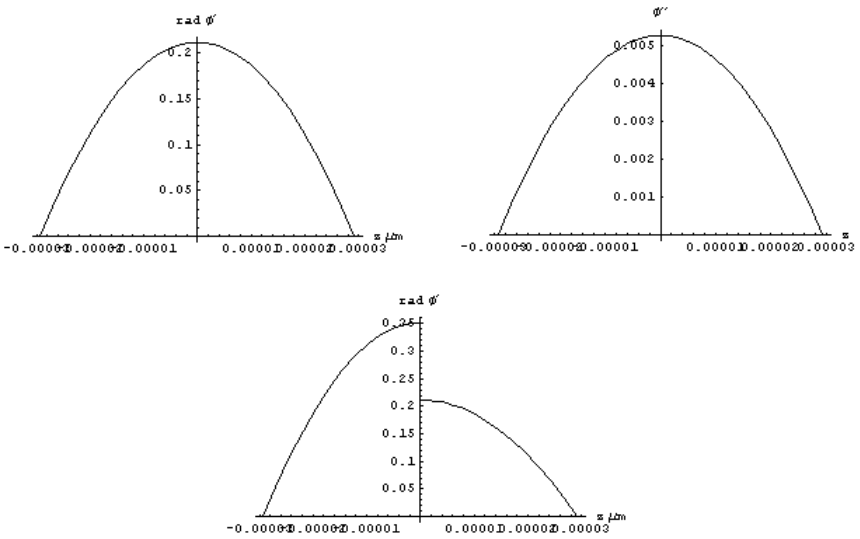


Figure 19: Theoretical Graphs of expected measurements. All the 1D plots are cuts at x=0 (on the trapping axis). The top left graph shows the dephasing and the top right the absorbency of the condensate. The bottom graph shows the dephasing for a condensate with one side atoms in the spin state $m_S = -3$ and on the other side $m_S = -2$.

# Conclusion

I presented the theory of dipole trapping and deduced the theoretical values of key parameters for our 2D dipole trap. We realize that our gas will not be purely 2D since the chemical potential is of the order of the trapping frequency along the strong confining axis $\sim$ 3kHz. We characterised the beam along the optical path and ascertain the fact that we produce a beam of 40$\mu$m horizontally and 10$\mu$m vertically. The dipole trap has been aligned and its characterisation will be performed in the coming days. At the same time, I prepared an imaging system, simulating our experimental conditions (i.e. with a piece of glass with a tilted angle to simulate the atoms chamber), of a resolution of 2.5$\mu$m. The imaging system was studied in depth, we concluded that the camera and the first and third lenses position is sensitive at the millimetre scale and will therefore be placed on a translational mount. The transverse field is experimentally of at least 400$\mu$m which is much larger than the size of our condensate. The depth of field was evaluated at the order of the Rayleigh length ($\sim$ 30$\mu$m). I designed mechanics for the imaging systems implementation. A phase spot was produced in order to perform the contrast phase imaging and characterized by profilmetre measurements, the spot has a diameter of 250$\mu$m and a height of 300 nm and should dephase the scattered beam by $\pi/2$. Finally a theoretical treatment of phase imaging technique was studied, and typical expected curves were given. From these graphs we can conclude that thanks to the extreme sensitivity of our new camera we will be able to perform phase contrast imaging of the atoms spin state. Unfortunately, by imaging, we will be a little absorptive and so the system will not be completely non destructive.

# Appendix: Clebsch-Gordan Coefficients

I present here the Clebsch-Gordan coefficients for the allowed transitions between $^{52}Cr$ ground state and its $^7P_4$ are shown figure 20. These are important since it is thanks to the difference between the coefficients that we will probe the different spin states.

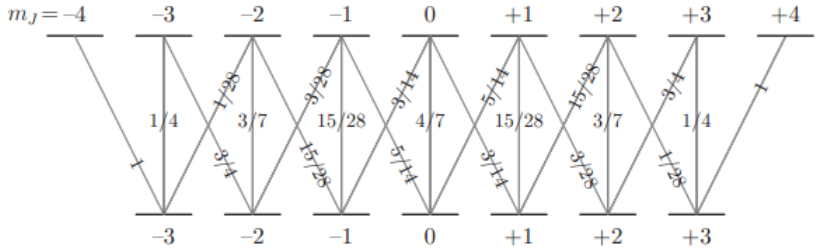


Figure 20: The squares of the Clebsch-Gordan coefficients for the allowed transitions between $^7S_3$ and $^7P_4$.


# Acknowledgement

I would like to thank the whole GQD team. Aurelie, Bruno, Etienne, and Laurent were always there to help me and explain things to me. Also I would like to thank them for listening to me : never have I felt so supported in a team. Villetaneuse is far, very far even, but the people and the topic of research are worth it.

# References


[1] A. Griesmaier, J. Werner, S. Hensler, J. Stuhler and T. Pfau, *Bose-Einstein Condensation of chromium*. Phys. Rev. Lett **94**, 160401 (2005).

[2] R. Chicireanu, Q. Beaufils, A. Pouderous, B. Laburthe-Tolra, E. Marechal, J. V. Porto, L. Vernac, J. C. Keller and O. Gorceix, *Simultaneous Magneto-Optical Trapping of Bosonic and Fermionic Chromium Atoms*. Phys. Rev. A **73**, 053406 (2006).

[3] Q. Beaufils, R. Chicireanu, T. Zanon, B. Laburthe-Tolra, E. Marechal, L. Vernac, J. -C. Keller and O. Gorceix, *All-Optical Production of Chromium Bose-Einstein Condensates*. Phys. Rev. A **77**, 061601 (2008).

[4] G. Bismut, B. Laburthe-Tolra, E. Maréchal, P. Pedri, O. Gorceix and L. Vernac, *Anisotropic excitation spectrum of a dipolar quantum Bose gas*. Phys. Rev. Lett **109**, 155302 (2012).

[5] G. Bismut, B. Pasquiou, E. Marechal, P. Pedri, L. Vernac, O. Gorceix and B. Laburthe-Tolra, *Collective Excitations of a Dipolar Bose-Einstein Condensate*. Phys. Rev. Lett. **105**, 040404 (2010).

[6] B. Pasquiou, E. Marechal, L. Vernac, O. Gorceix and B. Laburthe-Tolra, *Thermodynamics of a Bose-Einstein Condensate with Free Magnetization*. Phys. Rev. Lett **108**, 045307 (2012).

[7] B. Pasquiou, G. Bismut, E. Maréchal, P. Pedri, L. Vernac, O. Gorceix and B. Laburthe-Tolra, *Spin relaxation and Band excitation of a dipolar Bose-Einstein Condensate in 2D Optical Lattices*. Phys. Rev. Lett **106**, 015301 (2011).

[8] S. Chaudhuri, S. Roy, C.S. Unnikrishnnan, *Evaporative Cooling of Atoms to Quantum Degeneracy in an Optical Dipole Trap*. Journal of Phys. **80**, 012036 (2007).

[9] G. Rudolf, W. Matthias and Ovchinnikov Yurii B., *Optical dipole traps for neutral atoms*, Advances in Atomic, Molecular and Optical Physics, **42**, (2000).

[10] J.D. Jackson, *Classical electrodynamics* Wiley, New York (1962).

[11] L. Pitaevskii and S. Stringari, *Bose-Einstein Condensation*, Chap.5, Oxford University Press (2003).

[12] T. Lahaye, C. Menotti, L. Santos, M. Lewenstein, T. Pfau, *The physics of dipolar bosonic quantum gases*. Rep. Prog. Phys. 72, 126401 (2009)

[13] C.J. Pethick and H. Smith, *Bose-Einstein Condensation in Dilute Gases*, Chap.6, Cambridge University Press (2008).

[14] C.J. Pethick and H. Smith, *Bose-Einstein Condensation in Dilute Gases*, Chap.4, Cambridge University Press (2008).

[15] Y. Castin and R. Dum, *Bose Einstein Condensation in Time Dependant Traps*. Phys. Rev. Lett **77**, 5315 (1996).

[16] A. Pouderous, *Refroidissement et piegage d'atomes de Chrome* Ph.D. Thesis (2007).

[17] E. Maréchal, G. Bismut, P. Pedri, L. Vernac, O. Gorceix and B. Laburthe-Tolra, *Spontaneous demagnetization of a dipolar spinor Bose gas at ultra low magnetic field*. Phys. Rev. Lett **109**, 155302 (2012).

[18] J.W. Goodman., *Introduction to Fourier Optics.*, chap.4 , 2nd edition (1996).

[19] Alexander Franzen, *Inkscape*.

[20] W. Gerlach, O. Stern, *Das magnetische Moment des Silberatoms.*Zeitschrift fur Physik **9**, 353-355 (1922).

[21] F. Zernike, Month. Not. Roy. Astro. Soc. **94**,0377 (1933)

[22] S. Chu, J.E. Bjorkholm, A.Ashkin, and A. Cable, *Experimental Observation of Optically Trapped Atoms*. Phys. Rev. Lett. **57**, 3 (1986).

[23] T.A. Savard, K.M. O'Hara, and J.E. Thomas, *Laser-noise-induced heating in far-off resonance optical traps*, Phys. Rev. A **56**, 2 (1997).